Korean J. Chem. Eng., **31**(5), 905-910 (2014)
DOI: 10.1007/s11814-014-0046-y

pISSN: 0256-1115
eISSN: 1975-7220

Electrochemical properties of Co-less layered transition metal oxide as high energy cathode material for Li-ion batteries

Sungho Choo*,**, Hye Yeon Kim*, Dong Young Yoon*, Wonchang Choi*, Si-Hyung Oh*, Jeh Beck Ju**, Jang Myoun Ko***,†, Ho Jang****, and Won Il Cho*,†**

*Center for Energy Convergence, Korea Institute of Science and Technology, Seoul 136-791, Korea
**Department of Chemical Engineering, Hongik University, Seoul 121-791, Korea
***Department of Chemical and Biological Engineering, Hanbat National University, 125, Yuseong-gu, Daejeon 305-719, Korea
****Department of Materials Science and Engineering, Korea University, 145, Anam-ro, Seongbuk-gu, Seoul 136-701, Korea
(*Received 29 October 2013 • accepted 6 February 2014*)

Abstract–High energy nickel manganese cobalt oxide materials (HENMC) are one of the most viable cathode materials for a high energy density lithium ion battery (LIB), but they contain expensive and toxic cobalt (Co). We synthesized Co-free high energy nickel manganese oxide cathode materials (HENM) via a solid state reaction method and a co-precipitation method. Their structural and electrochemical properties were comparatively investigated using X-ray diffraction spectroscopy (XRD), scanning electron microscopy (SEM), inductively coupled plasma (ICP), electron probe micro-analysis (EPMA), particle size analysis (PSA) and electrochemical impedance spectroscopy (EIS). The co-precipitated HENM and the solid state fabricated HENM showed high capacities of 250 $mAhg^{-1}$ and 240 $mAhg^{-1}$, respectively. It suggests that the solid state fabricated method of HENM would be a good candidate for practical application as well as the co-precipitated one.

Keywords: Li Ion Battery, High Capacity, Cathode, Nickel Manganese Oxide, Solid State Method, Co-precipitation

INTRODUCTION

The lithium ion battery (LIB) is one of the most advanced rechargeable batteries in the commercial battery market and its high energy density, light weight, and better cycle performance make it useful for applications in various areas, from cell phones and notebook PCs to extended electric vehicles (xEV) and energy storage systems (ESS) [1].

Even though both cathode and anode materials with high specific capacity are very critical for the development of LIB for high energy density applications, there are no commercially available high capacity cathode materials except for lithium nickel manganese cobalt oxide (NMC) and lithium nickel cobalt aluminum oxide (NCA). To develop novel cathode materials with a capacity higher than 200 $mAhg^{-1}$, many researchers have investigated various types of materials including Li_2MnSiO_4 [2], $LiFeF_3$ [3], $(1-z)Li[Li_{1/3}Mn_{2/3}]O_2 \cdot zLi[Mn_{0.5-y}Ni_{0.5-y}Co_{2y}]O_2$ (high energy lithium nickel manganese cobalt oxide, HENMC) [4-15], and $xLi[Mn_{1.5}Ni_{0.5}]O_4 \cdot (1-x)\{Li_2MnO_3 \cdot Li(Mn_{0.5}Ni_{0.5})O_2\}$ (high energy lithium nickel manganese oxide, HENM) [4-7,16,17]. Among them, the HENMC has been known to work at a high potential of 4.9 V vs. Li/Li+ and to show a capacity of more than 250 $mAhg^{-1}$ [4-7]. However, they have critical problems such as poor rate capability, large irreversibility of the first cycle, and a continuous decrease of the discharge voltage plateau during cycling, which should be overcome for its practical use in xEV or ESS.

The cobalt-free HENM has been fabricated by using a co-precipitation process similar to the process used to make the NMC [16, 17]. The HENM behaves similarly to HENMC, but its structural stability may be decreased due to the absence of cobalt atoms in the lattice. Nevertheless, this cobalt free cathode is very attractive because of the lack of expensive cobalt.

We synthesized the HENMs employing co-precipitation method and analyzed their structural and electrochemical properties. After that, the samples of same composition were prepared based on the solid state reaction process, and their electrochemical and physical properties were comparatively studied, including their crystal structure, elements distribution, morphology, particle size distribution, cycle performance, rate capability, and charge transfer resistance.

EXPERIMENTAL

1. Sample Preparation

$0.5Li_2MnO_3 \cdot 0.5LiNi_{0.5}Mn_{0.5}O_2$ powder (s-HENM) obtained by a solid state reaction was prepared as follows: First, the monoclinic Li_2MnO_3 was prepared by ball milling $MnCO_3$ and Li_2CO_3, followed by heat treatment at 500 °C for 72 h in air. Second, NiO+MnO_2 and LiOH were subjected to ball milling and heat treatment at 1,000 °C for 12 h in air to obtain $LiNi_{0.5}Mn_{0.5}O_2$. Finally, the $LiNi_{0.5}Mn_{0.5}O_2$ and Li_2MnO_3 powders were mixed via ball milling with the same stoichiometric ratio; then, the mixture was heat treated at 900 °C for 6 h in air.

†To whom correspondence should be addressed.
E-mail: wonic@kist.re.kr, jmko@hanbat.ac.kr

We prepared the $0.5Li_2MnO_3 \cdot 0.5LiNi_{0.5}Mn_{0.5}O_2$ (c-HENM) by using a co-precipitation process for precursors and solid state reaction as follows: a 0.1 M aqueous solution of $MnSO_4$ and $NiSO_4$ with a 1 : 3 molar ratio, and a 1 M aqueous solution of $NaHCO_3$ were injected into a glass reactor to precipitate the precursor $Ni_{0.25}Mn_{0.25}CO_3$ with a stirring speed of 250 rpm. The co-precipitated precursor was washed several times and dried at 80 °C for one day. Li_2CO_3 was mixed with the $Ni_{0.25}Mn_{0.25}CO_3$, and the mixture was heat-treated at 900 °C for 6 h in air.

2. XRD, SEM, EPMA, PSA and TGA

s-HENM and c-HENM were investigated using XRD (Rigaku D/max-II), SEM (Nova nano SEM 2000), EPMA (JEOL JXA-8500F) and particle size analyzer (Micromeritics Saturn DigiSizer II). X-ray diffraction patterns were obtained from 2θ=10° to 80° with a scanning rate of 0.3°/min, and the applied current and voltage to generate X-rays (Cu K-α line) were 100 mA and 40 kV, respectively.

3. Cell Assembly and Test

Cathodes were made by mixing the prepared $0.5Li_2MnO_3 \cdot 0.5LiNi_{0.5}Mn_{0.5}O_2$, acetylene black, and polyvinylidene difluoride at a ratio of 8 : 1 : 1. The slurry mixture was coated on an Al foil using a doctor blade and dried at 80 °C for 24 h. The coated and dried electrode was punched to make a circular 16 mm diameter disk with the surface area of 2.0 cm^2. The cathode was 80 μm thick and it contained approximately 11-12 $mg \cdot cm^2$ of active material. The charge and discharge characteristics of the cathodes were examined using coin cells (2032 type). The cells consisted of a cathode, an electrolyte, a lithium metal anode, and a Celgard 2500 separator. The electrolyte was a 1 M $LiPF_6$-ethylene carbonate/dimethyl carbonate/ethylmethyl carbonate (EC/DMC/EMC) solution. The galvanostatic charge-discharge experiments were performed between 2.0 and 4.9 V using a Maccor 4000 battery cycler. The rate capability was also tested by applying various discharge currents of 0.05 C-2 C for 5 cycles step, applying 0.05 C discharge current after each step and 0.05 C rate was kept during every charge procedures. Electrochemical impedance spectroscopy (EIS) was carried out in the frequency range of 100 kHz to 1 mHz with an AC-amplitude of 10 mV (Multi electrochemical analyzer system VSP, BioLogic).

RESULTS AND DISCUSSION

1. Structure and Morphology of HENM

Fig. 1(a) shows the XRD data of the Li_2MnO_3 which can be indexed as a well-known Li_2MnO_3 monoclinic structure. The Li_2MnO_3 structure has been reported to be trigonal ($P3_112$) [18] as well as monoclinic, either C2/m [19-21] or C2/c [22]. The diffracted peaks of approximately 21 degrees marked as "★" in the Fig. 1(a) were previously reported to originate from the super lattice structure composed of the Li_2MnO_3 phase [23]. The super lattice diffraction patterns of (020), (110), ($\bar{1}$11), (021), and (111) are not clearly shown in the Fig. 1(a) due to the low calcination temperature of 500 °C.

The XRD of the s-HENM is shown in Fig. 1(b), which is well indexed to the α-$NaFeO_2$ structure with the space group $R\bar{3}m$ [24]. Fig. 1(c) shows the XRD data of the s-HENM representing the layered structure of $LiNi_{0.5}Mn_{0.5}O_2$ with the super lattice peaks of Li_2MnO_3 between 2θ=20°-25°, suggesting that the s-HENM can be expressed by the two layered components as $0.5Li_2MnO_3 \cdot 0.5LiNi_{0.5}Mn_{0.5}O_2$ [25]. The XRD result of the c-HENM is shown in Fig. 1(d). The peak positions of the XRD result are the same as for s-HENM, which implies the two layered structure of $0.5Li_2MnO_3 \cdot 0.5LiNi_{0.5}Mn_{0.5}O_2$.

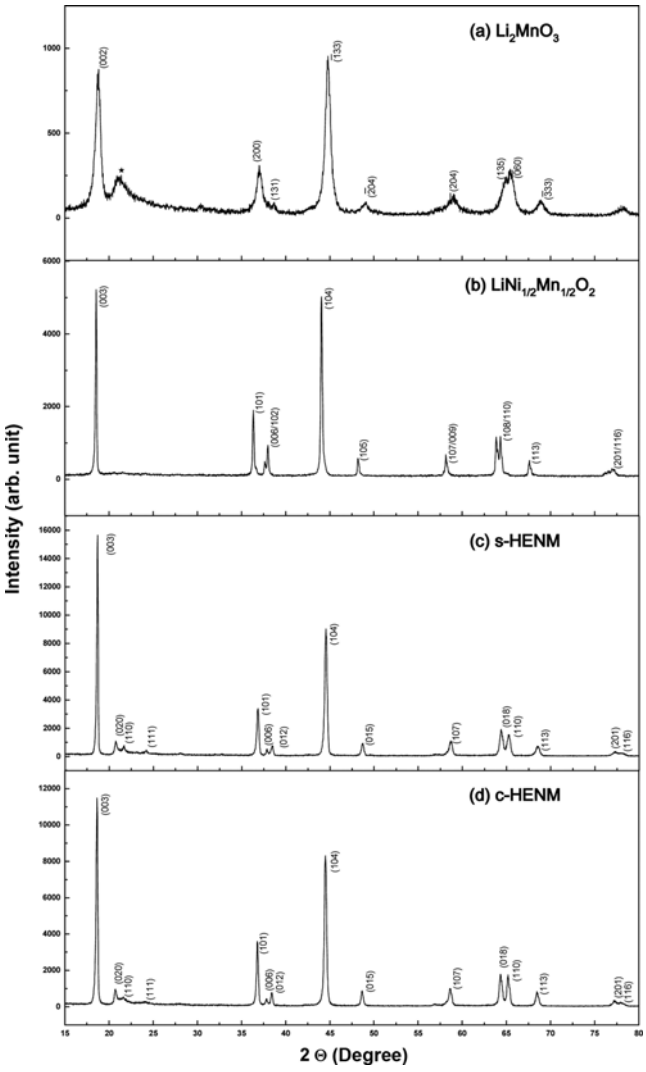

Fig. 1. X-ray diffraction results of (a) Li_2MnO_3, (b) $LiNi_{0.5}Mn_{0.5}O_2$, (c) s-HENM, and (d) c-HENM.

It was previously reported that the XRD intensity ratio I_{104}/I_{003} between (104) and (003) in the $R\bar{3}m$ space group increases with the displacement between the cations sitting on the 3a and 3b sites [27], which means that the higher XRD intensity ratio, the lesser cationic disorder. Our XRD results in Fig. 1(c) and (d) show that the I_{104}/I_{003} of the s-HENM and the c-HENM are 0.59 and 0.62, respectively.

Fig. 2(a) and (b) display the surface morphologies of s-HENM and c-HENM, showing the irregular shape of s-HEHM powder and the spherical shape of c-HENM powder, which would be better for electrode fabrication. EPMA photographs in the boxes shown in Fig. 2(a) and (b) show little difference of nickel and manganese element and give weak evidence of better compositional uniform distribution obtained from c-HENM. In general, powders with well-distributed metal ions could not be easily synthesized for the bigger particles compared to the smaller particles. The s-HENM particles exhibited well distributed metal ions by EPMA as expected and interestingly, c-HENM samples with over 7 μm diameter also show

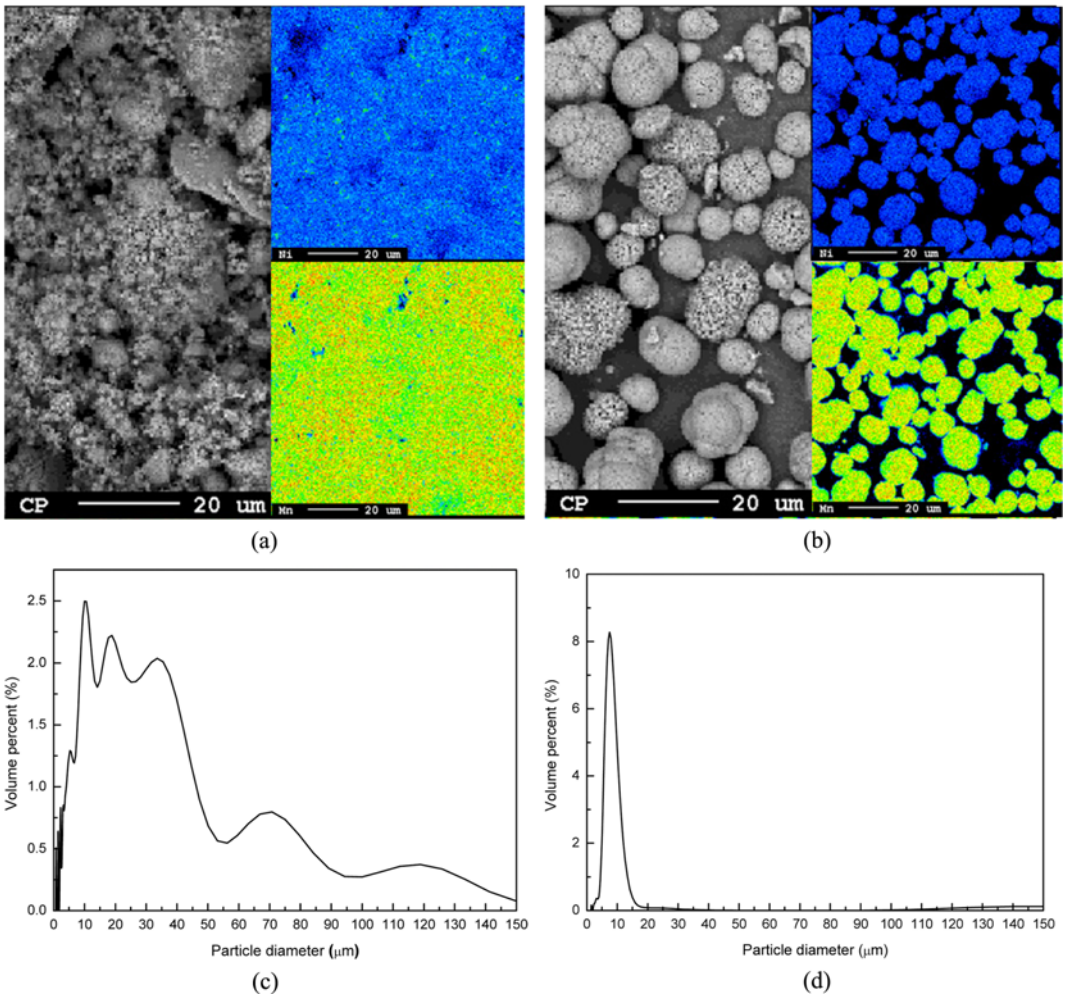

Fig. 2. SEM images of (a) s-HENM and (b) c-HENM and their particle size distribution (PSA) (c) s-HENM and (d) c-HENM.

a homogeneous distribution of nickel and manganese element. It suggests that the co-precipitation method can be effective to obtain the well-controlled powders. We identified the atomic compositions of the c-HENM and s-HENM, which were $Li_{1.200}Ni_{0.194}Mn_{0.603}O_{2.003}$ and of $Li_{1.200}Ni_{0.191}Mn_{0.607}Mn_{0.607}O_{2.002}$, respectively. These values are very close to the stoichiometric oxidation of $Li_{1.2}Ni_{0.2}Mn_{0.6}O_2$. The particle size distribution of s-HENM is shown to be different from that of c-HENM in Fig. 2(a) and (b), respectively. We obtained the particle size distribution of the s-HENM and c-HENM samples via particle size analysis, as shown in Fig. 2(c) and (d), respectively. The particle size of the s-HENM is rather widely distributed from 0.1 μm to 150 μm with an average size of approximately 15.8 μm, while the c-HENM has a relatively narrower distribution with a smaller average size of approximately 7.6 μm. The particle size data suggests that one of the critical factors related to the specific capacity of the 1st cycle in the Li_2MnO_3 is particle size [29].

2. Electrochemical Properties of HENM

Eqs. (1) and (2) show the intercalation and the deintercalation reaction of HENM with lithium. The Li_2MnO_3 is decomposed at 1st charge and its theoretical capacity is 344 $mAhg^{-1}$. The reversible reaction represented by Eq. (2) corresponds to the inter/deintercalation of the $LiNi_{0.5}Mn_{0.5}O_2$ and it is associated with a theoretical capacity of 280 $mAhg^{-1}$.

$$Li_2MnO_3 \rightarrow Li^+ + 0.5Li_2O + MnO_2 + 1/2\ O_2\ (\text{only } 1^{st} \text{ charge})/344\ mAhg^{-1} \quad (1)$$

$$LiNi_{0.5}Mn_{0.5}O_2 \leftrightarrow Li^+ + Ni_{0.5}Mn_{0.5}O_2 + e^-/280\ mAhg^{-1} \quad (2)$$

Fig. 3 shows the charge and discharge curves of s-HENM and c-HENM at the 1st, 2nd, 5th, 10th cycles, which were charged up to 4.9 V. Two types of the samples exhibit a plateau near the 4.5 V in the first charge profile, representing the decomposition of the Li_2MnO_3 phase into $Li+0.5Li_2O_2+MnO_2$, as reported previously [16,17]. In the subsequent charge and discharge profiles shown by Fig. 3(b)-(d), the plateau around 4.5 V is absent, indicating that the oxygen loss during the first charge is an irreversible process. Moreover, it is certain that the decomposition of electrolyte also causes the irreversible capacity when the cells are charged up to 4.65 V [32].

As the particle size decreases, more oxygen ions are released during the 1st cycle [27]. Therefore, we can expect that the smaller specific capacity of the 1st cycle in the s-HENM would come from the large particle size distribution with particles up to 100 μm because large particle sizes give relatively smaller specific capacity.

As cycles continue, the capacity and voltage profiles of c-HENM become similar to that of s-HENM, but one significant change which is exhibited to all samples stands out. The starting point of oxidation between Ni^{2+} and Ni^{4+} more and more drops from 3.5 V to 3.0 V,

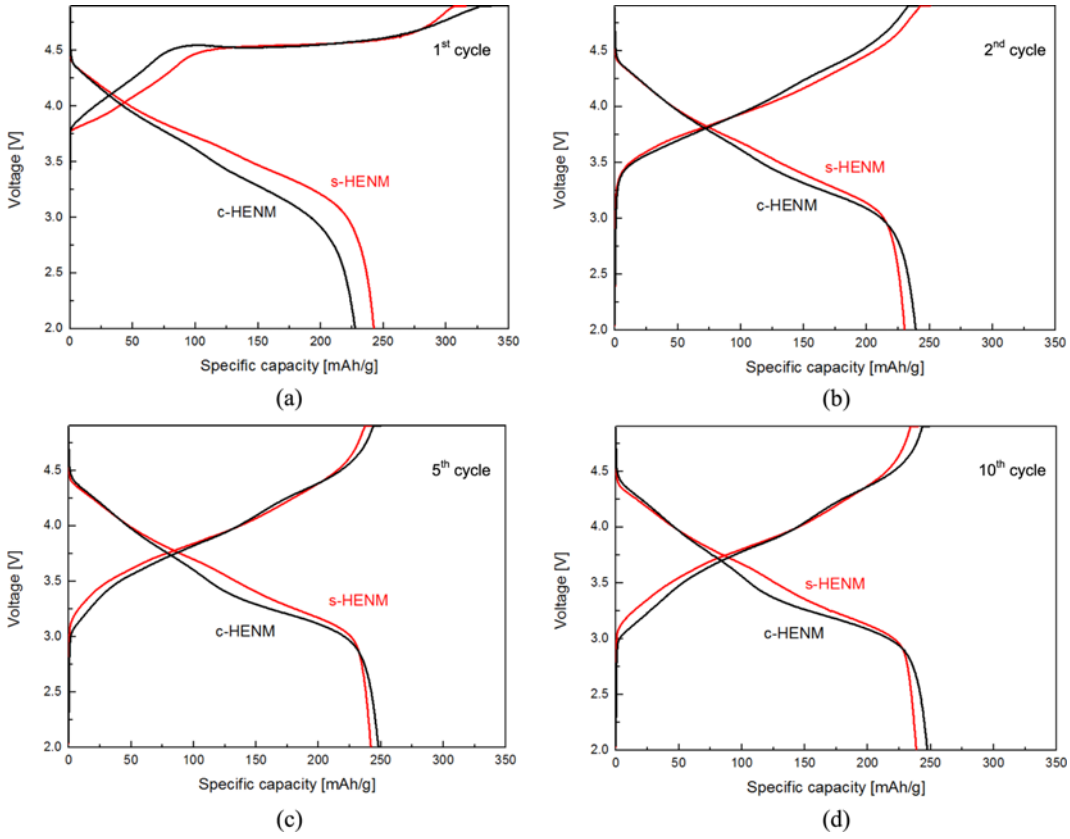

Fig. 3. The voltage profile of the s-HENM and c-HENM for the (a) 1st cycle, (b) 2nd cycle, (c) 5th cycle and (d) 10th cycle.

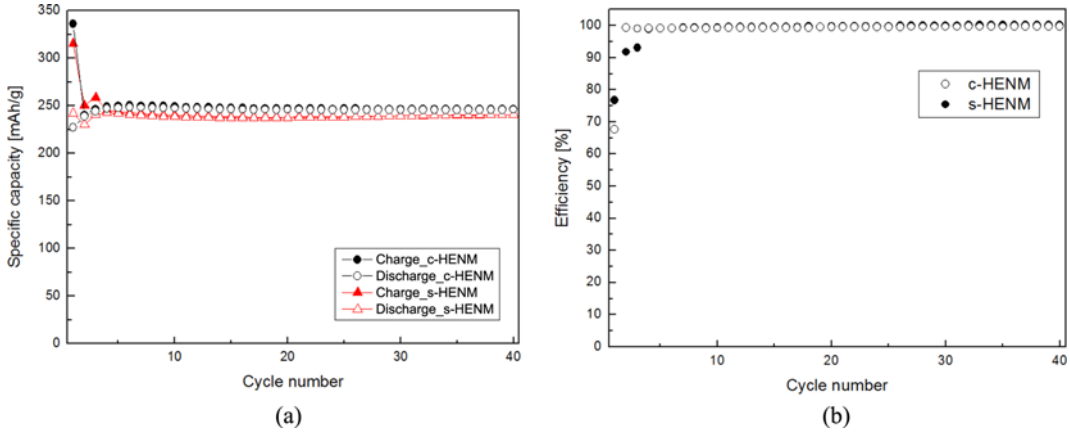

Fig. 4. (Color online) (a) Open and solid circles represent the charge and discharge capacities of the c-HENM with cycle, respectively. Open and solid triangles represent those of the s-HENM with cycle, respectively. (b) Open and solid circles represent the cycle efficiencies of the discharge capacities of the c-HENM and s-HENM, respectively.

as shown by Fig. 3(b)-(d), representing that the electrochemical activity gradually develops in the charge from 2nd to 10th cycle [31].

Cycle performance and charge-discharge efficiency of the s-HENM and c-HENM are shown in Fig. 4(a) and (b), respectively. The discharge capacity of both the s-HENM and the c-HENM is in the range of 240-250 $mAhg^{-1}$ at the discharge rate of 0.1 C after a couple of cycles. It shows that the obtained experimental value is lower than the theoretical capacity which is shown by Eq. (2). The reason for low capacity in comparison with the theoretical capacity is that the inter/deintercalation of the $LiNi_{0.5}Mn_{0.5}O_2$ exclusively happened since the 2nd cycle, as shown by Fig. 3(a)-(d). In addition, this value was similar to 244 $mAhg^{-1}$ and higher than 238 $mAhg^{-1}$, as Sun et al. [30] and Kang et al. [31] reported, respectively. The charge-discharge efficiencies became constant after the 4th cycle. The efficiency of s-HENM goes down to below 90% until the 3rd cycle and reaches 99% after the 4th cycle due to its relatively lower homogeneity than c-HENM. The efficiency of the c-HENM after the 4th cycle is slightly better than that of the s-HENM.

The rate capabilities and impedance of both cathode materials were measured and are shown in Fig. 5 and Fig. 6, respectively. The

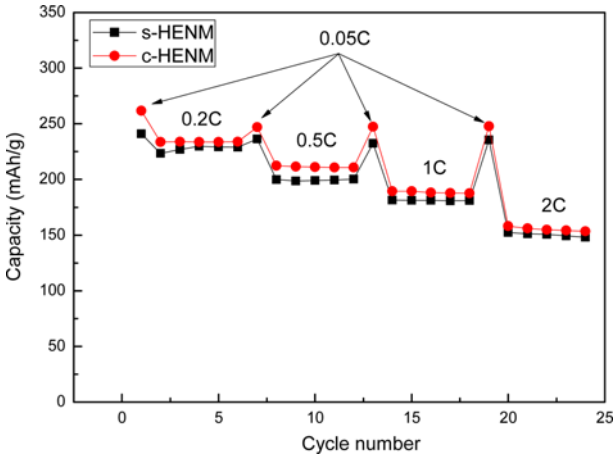

Fig. 5. The rate capabilities of s-NENM and c-HENM depending on various discharge rates.

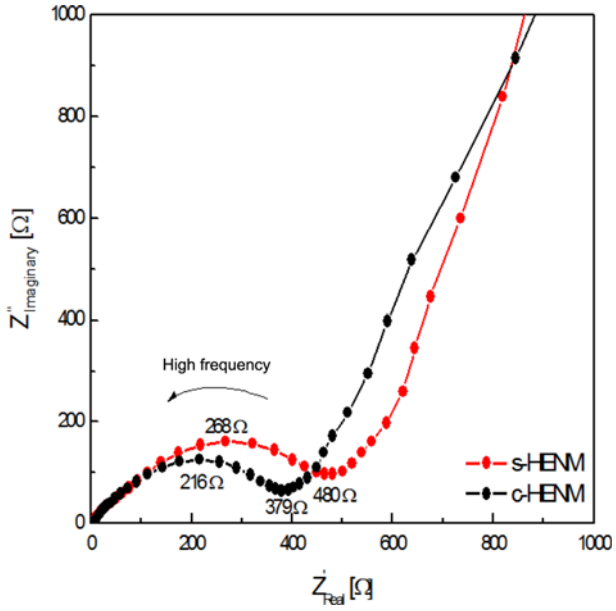

Fig. 6. Impedance spectra of fresh half cells with s-HENM and c-HENM, respectively.

rate performance of c-HENM is better than that of s-HENM at the rates from 0.05 C to 2 C and specifically at the rate 0.5 C. The uniform size distribution of c-HENM around 7 μm may contribute to a better rate capability, while the rate performance difference is reduced at both high rates of 1 C and 2 C. Electrochemical impedance spectroscopy (EIS) was carried out at the fresh state of both samples. The calculated surface layer resistance (R_{sl}) of the s-HENM and the c-HENM is 460 Ω and 370 Ω, which are observed in the semicircles presented in Fig. 6. In other words, the charge transfer reaction at the interface of c-HENM and electrolyte solution is somehow enhanced than that of s-HENM and electrolyte solution, which is in agreement with the fact that the electrochemical performance of the c-HENM is slightly better than that of the s-HENM. But there is no large difference in the electrode performance to suggest that the solid state fabricated method of HENM would be a good candidate for practical application as well as the co-precipitated one.

CONCLUSION

To understand the difference of battery performance for the HENM prepared in two different methods, namely solid state reaction and co-precipitation process, comparative studies were carried out. Less cationic disorder in the c-HENM than in the s-HENM is one of the causes of the improved cycle performance and rate capability. The c-HENM, having a narrower range of particle size distribution and uniform compositional distribution, reveals somewhat better electrochemical performance than the s-HENM. But there is no large difference in the electrode performance to suggest that the solid state fabricated method of HENM would be a candidate for practical application as well as the co-precipitated one.

ACKNOWLEDGEMENTS

This work was supported by the Energy Efficiency & Resources program of the Korea Institute of Energy Technology Evaluation and Planning (KETEP) grant funded by the Korea government Ministry of Knowledge Economy (2011201010016C, 20102010100090-11-2-200 and 20118510010030).

REFERENCES

1. B. L. Ellis, K. T. Lee and L. F. Nazar, *Chem. Mater.*, **22**, 691 (2010).
2. F. Dominko, M. Bele, M. Gaberscek, A. Meden, M. Remskar and M. Jamnik, *Electrochem. Commun.*, **8**, 217 (2006).
3. R. E. Doe, K. A. Persson, Y. S. Meng and G. Ceder, *Chem. Mater.*, **20**, 5274 (2008).
4. S.-H. Kang, P. Kempgens, S. Greenbaum, A. J. Kropf, K. Amine and M. M. Thackeray, *J. Mater. Chem.*, **17**, 2069 (2007).
5. M. M. Thackeray, S.-H. Kang, C. S. Johnson, J. T. Vaughey, R. Benedek and S. A. Hackney, *J. Mater. Chem.*, **17**, 3112 (2007).
6. C. S. Johnson, N. Li, C. Lefief, J. T. Vaughey and M. M. Thackeray, *Synth. Chem. Mater.*, **20**, 6095 (2008).
7. S.-H. Kang, W. Lu, K. G. Gallagher, S.-H. Park and V. G. Pol, *J. Electrochem. Soc.*, **158**, A936 (2011).
8. G.-Y. Kim, S.-B. Yi, Y. J. Park and H.-G. Kim, *Mater. Res. Bull.*, **43**, 3543 (2008).
9. Q. Y. Wang, J. Liu, A. V. Murugan and A. Manthiram, *J. Mater. Chem.*, **19**, 4965 (2009).
10. A. Ito, D. Li, Y. Sato, M. Arao, M. Watanabe, M. Hatano, H. Horie and Y. Ohsawa, *J. Power Sources*, **195**, 567 (2010).
11. X. Zhang, W. J. Jiang, A. Mauger, Qilu, F. Gendron and C. M. Julien, *J. Power Sources*, **195**, 1292 (2010).
12. J. Liu and A. Manthiram, *J. Mater. Chem.*, **20**, 3961 (2010).
13. J. Liu, B. Reeja-Jayan and A. Manthram, *J. Phys. Chem. C*, **114**, 9528 (2010).
14. J. Liu, Q. Wang, B. Reeja-Jayan and A. Manthram, *Electrochem. Commun.*, **12**, 750 (2010).
15. F. Amalraj, D. Kovacheva, M. Talianker, L. Zeiri, J. Grinblat, N. Leifer, G. Gobes, B. Markovsky and D. Aurbach, *J. Electrochem. Soc.*, **157**, A1121 (2010).
16. S. H. Park, S.-H. Kang, C. S. Johnson, K. Amine and M. M. Thackeray, *Electrochem. Commun.*, **2**, 262 (2007).
17. J. Cabana, S.-H. Kang, C. S. Johnson, M. M. Thackeray and C. P. Grey, *J. Electrochem.Soc.*, **156**, A730 (2009).

18. Y. S. Meng, G. Ceder, C. P. Grey, W. S. Yoon, M. Jiang, J. Breger and Y. Shao-Horn, *Chem. Mater.*, **17**, 2386 (2005).
19. J. Breger, M. Jiang, N. Dupre, Y. S. Meng, Y. Shao-Horn, G. Ceder and C. P. Grey, *J. Solid State Chem.*, **178**, 2575 (2005).
20. V. Massarotti, M. Bini, D. Capsoni, A. Altomare and A. G. G. Moliterni, *J. Appl. Crystallogr.*, **30**, 123 (1997).
21. P. Strobel and B. Lambertandron, *J. Solid State Chem.*, **75**, 90 (1988).
22. A. Riou, A. Lecerf, Y. Gerault and Y. Cudennec, *Mater. Res. Bull.*, **27**, 269 (1992).
23. A. Boulineau, L. Croguennec, C. Delmas and F. Weill, *Solid State Ionics*, **180**, 1652 (2010).
24. T. Ohzuku and Y. Makimura, *Chem. Lett.*, **7**, 642 (2001).
25. H. Deng, I. Belharouak, R. E. Cook, H. Wu, Y.-K. Sun and K. Amine, *J. Electrochem. Soc.*, **157**, A447 (2010).
26. H.-R. Seo, E.-A. Lee, C.-W. Yi and K.-O. Kim, *J. Electrochem. Sci. Technol.*, **3**, 180 (2011).
27. Y. Makimura and T. Ohzuku, *J. Power Sources*, **119**, 156 (2003).
28. P. Y. Liao, J. G. Duh and H. S. Sheu, *J. Power Sources*, **183**, 766 (2008).
29. D. Y. W. Yu, K. Yanagida, Y. Kato and H. Nakamura, *J. Electrochem. Soc.*, **156**, A417 (2009).
30. D.-K. Lee, S.-H. Park, K. Amine, H. J. Bang, J. Parakash and Y.-K. Sun, *J. Power Sources*, **162**, 1346 (2006).
31. J. H. Hong, D.-H. Seo, S.-W. Kim, H. J. Gwon, S.-T. Oh and K. S. Kang, *J. Mater. Chem.*, **20**, 10179 (2010).
32. Z. Lu and J. R. Dahn, *J. Electrochem. Soc.*, **149**, A815 (2002).